EPR-ENDOR of the Electronic Structure from Two Nitrogenously Ligated Bis(μ-oxo)-Mn^{III}-Mn^{IV} Model Complexes Spectroscopically Relevant to the Multi-Manganese Center of Photosystem II

Xiao-ling Tan,[†] Yilma Gultneh,[‡] Joseph E. Sarneski,[§] and Charles P. Scholes*,[⊥]

Contribution from the Department of Physics, Center for Biochemistry and Biophysics, and Department of Chemistry, State University of New York at Albany, Albany, New York 12222, Department of Chemistry, Howard University, 2400 Sixth Street, Northwest, Washington, D.C. 20059, and Department of Chemistry, Fairfield University, Fairfield, Connecticut 06430. *Received March 7, 1991*

Abstract: ENDOR (electron nuclear double resonance) gave hyperfine couplings to nitrogen(s) on the bis(μ-oxo)-Mn^{III}-Mn^{IV} complexes of CYCLAM (1,4,8,11-tetraazacyclotetradecane) and TMPA (tris(2-methylpyridyl)amine). PFSEPR (pulse field-sweep EPR) gave nitrogen hyperfine couplings consistent with the ENDOR results. The nitrogen hyperfine couplings from ENDOR were 9.2 MHz for CYCLAM and 11.2 MHz for TMPA. We provide justification that these couplings are due to a Fermi contact interaction with nitrogen 2s electron spin density at the axial nitrogens on the Mn^{III}, where this electron spin is contained in an antibonding e_g orbital along the Mn^{III}-nitrogen bond. The relevant axial nitrogen ligands are secondary amine nitrogens in the case of CYCLAM and pyridyl nitrogens in the case of TMPA. Compared to quadrupolar couplings from unligated secondary amine or pyridine, the quadrupolar interaction for both types of nitrogen indicated a significant decrease in electric field gradient at the nitrogen nucleus due to interaction of the nitrogen lone pair with the manganese. Proton ENDOR showed exchangeable protons associated with the CYCLAM complex but not with the TMPA complex. We assign these exchangeable CYCLAM protons on the basis of their large 6.7-MHz hyperfine coupling as exchangeable protons on the secondary amine nitrogens at the Mn^{III}.

The oxygen-evolving center (OEC[1]) of Photosystem II (PS II) in green plants accumulates oxidizing equivalents in one-electron steps. These steps are driven by absorption of individual light quanta at the PS II reaction center. Separate intermediate oxidation states called S states[2] correlate with light-induced removal of four electrons by four light quanta and subsequent generation of molecular oxygen.[3] Following the light-induced removal of one electron from dark-adapted PS II to give state S_2, a multiline EPR spectrum emerges that is characteristic of an oxidized form of the terminal donor in PS II.[4] Manganese is essential for generation of these states and for the oxidation of H_2O to O_2. Each PS II reaction center contains four manganese atoms.[5a,b]

Simulations of EPR spectra and comparison to synthetic manganese complexes have identified the S_2 spectrum, and thus the terminal donor, with a cluster of at least two and probably four manganese atoms.[4,6a,b,7] An important aspect of various models, especially in predicting the hyperfine splittings of the multiline spectrum, has been the need for tightly coupled Mn^{III}-Mn^{IV} pairs to heavily influence the EPR properties of the multiline S_2 state.[6a-c,7,9] To explain completely the multiline spectrum of the OEC and the concomitant $g = 4.1$ broad signal, a common tetranuclear origin has been suggested where the conversion between the multiline and the $g = 4.1$ signal is due to a relatively minor variation in exchange coupling.[7] The extensive hyperfine structure recently reported from the $g = 4.1$ signal argues for a tetranuclear origin.[8] The simplest and most extensively studied models for this S_2 state are bis(μ-oxo)-bridged Mn^{III}-Mn^{IV} models with nitrogenous ligands, starting chronologically with the bipyridyl complex[10,11] and progressing to more elaborate polydentate complexes such as those studied here.[12-14] The X-ray spectroscopy of the manganese atoms in PS II bears similarity to that of a bis(μ-oxo)-bridged Mn^{III}-Mn^{IV} dimer, suggesting (μ-oxo)-bridged manganese as a component of the OEC.[15,16]

A 16-line EPR pattern has been seen from bis(μ-oxo)-Mn^{III}-Mn^{IV} models[11,12] and has been simulated on the basis of two manganese nuclei (^{55}Mn has a nuclear spin = $^5/_2$), one with

[†] Department of Physics and Center for Biochemistry and Biophysics, State University of New York at Albany.
[‡] Howard University.
[§] Fairfield University.
[⊥] Department of Chemistry and Center for Biochemistry and Biophysics, State University of New York at Albany.

(1) Abbreviations: ENDOR, electron nuclear double resonance; ESEEM, electron spin echo envelope modulation; PFSEPR, pulse field-sweep EPR; OEC, oxygen-evolving center; PS II, photosystem II; TMPA, tris(2-methylpyridyl)amine, also called TPA in refs 14 and 24; CYCLAM, 1,4,8,11-tetraazacyclotetradecane, also called 14-aneN_4 in refs 13 and 14; μW, microwatt; G, gauss = 10^{-4} Tesla; ptp, peak to peak; S_1, S_2, S, the spin operators respectively for spin-2 Mn^{III}, spin-$^3/_2$ Mn^{IV}, and the coupled spin-$^1/_2$ Mn^{III}-Mn^{IV}-bis(μ-oxo) complex.

(2) Kok, B.; Forbush, B.; McGlorin, M. P. *Photochem. Photobiol.* **1970**, *11*, 457-475.
(3) Brudvig, G. W.; Beck, W.; De Paula, J. C. *Annu. Rev. Biophys. Biophys. Chem.* **1989**, *18*, 25-46.
(4) Dismukes, G. C.; Siderer, Y. *Proc. Natl. Acad. U.S.A.* **1981**, *78*, 274-278.
(5) (a) Cheniae, G. M.; Martin, I. F. *Biochim. Biophys. Acta* **1970**, *197*, 219-239. (b) Yocum, C. F.; Yerkes, C. T.; Blankenship, R. E.; Sharp, R. R.; Babcock, G. T. *Proc. Natl. Acad. Sci. U.S.A.* **1981**, *78*, 7507-7511.
(6) (a) DePaula, J. C.; Brudvig, G. W. *J. Am. Chem. Soc.* **1985**, *107*, 2648-2654. (b) DePaula, J. C.; Beck, W. F.; Brudvig, G. W. *J. Am. Chem. Soc.* **1986**, *108*, 4002-4009. (c) DePaula, J. C.; Beck, W. F.; Miller, A-F.; Wilson, R. B.; Brudvig, W. *J. Chem. Soc., Faraday Trans. 1* **1987**, *83*, 3635-3651.
(7) Brudvig, G. W. In *Advanced EPR Applications in Biology and Biochemistry*; Hoff, A. J., Ed.; Elsevier: Amsterdam, 1989; pp 839-863.
(8) Kim, D. H.; Britt, R. D.; Klein, M. P.; Sauer, K. *J. Am. Chem. Soc.* **1990**, *112*, 9389-9391.
(9) Haddy, A.; Aasa, R.; Andréasson, L-E. *Biochemistry* **1989**, *28*, 6954-6959.
(10) Plaskin, P. M.; Stoufer, R. C.; Mathew, M.; Palenik, G. J. *J. Am. Chem. Soc.* **1972**, *94*, 2121-2122.
(11) Cooper, S. R.; Dismukes, G. C.; Klein, M. P.; Calvin, M. *J. Am. Chem. Soc.* **1978**, *100*, 7248-7252.
(12) Brewer, K. J.; Liegevis, A.; Otvos, J. W.; Calvin, M.; Spreer, L. O. *J. Chem. Soc., Chem. Commun.* **1988**, 1219-1220.
(13) Brewer, K. J.; Calvin, M.; Lumpkin, R. S.; Otvos, J. W.; Spreer, L. O. *Inorg. Chem.* **1989**, *28*, 4446-4451.
(14) Towle, D. K.; Botsford, C. A.; Hodgson, D. J. *Inorg. Chim. Acta* **1988**, *141*, 167-168.
(15) Yachandra, V. K.; Guiles, R. D.; McDermott, A. E.; Britt, R. D.; Dexheimer, S. L.; Sauer, K.; Klein, M. P. *Biochim. Biophys. Acta.* **1986**, *850*, 324-332.
(16) Yachandra, V. K.; Guiles, R. D.; McDermott, A. E.; Cole, J. L.; Britt, R. D.; Dexheimer, S. L.; Sauer, K.; Klein, M. P. *Biochemistry* **1987**, *26*, 5974-5978.

0002-7863/91/1513-7853$02.50/0

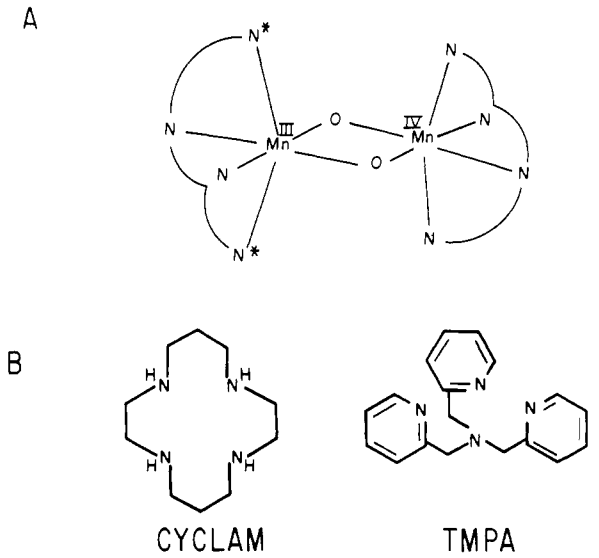

Figure 1. (A) Schematic of the liganding environment of the bis(μ-oxo)-Mn^{III}-Mn^{IV} center in the models studied. The asterisks denote the nitrogens with the longest metal-nitrogen bonds that have been distorted by a Jahn-Teller effect. (B) CYCLAM (1,4,8,11-tetraazacyclotetradecane) and TMPA (tris(2-methylpyridyl)amine).

a hyperfine coupling of about 160 G and the other with a hyperfine coupling of about 80 G. The manganese hyperfine splittings and g values for such complexes bear considerable resemblance to those of the S_2 state. They also bear considerable resemblance to splittings observed for dimanganese catalase.[17] In the bis(μ-oxo)-Mn^{III}-Mn^{IV} models, the spin = 2 (S_1 = 2) Mn^{III} and spin = $^3/_2$ (S_2 = $^3/_2$) Mn^{IV} are antiferromagnetically coupled to yield a net spin = 1/2 (S = $^1/_2$). For the Mn^{III}-Mn^{IV} dimer, the spin-coupled model[11,18,19] discussed below explains why the effective hyperfine coupling to the Mn^{III} nucleus should be twice its value on isolated Mn^{III} complexes and why the effective hyperfine coupling of the Mn^{IV} should be the negative of its value on isolated Mn^{IV} complexes. The two *distinct* hyperfine couplings for Mn^{III} and Mn^{IV}, as found in the bis(μ-oxo)-Mn^{III}-Mn^{IV} complexes, are consistent with localized, trapped Mn^{III} and Mn^{IV} valences[20] rather than a mixed valence system in which the manganese atoms are electronically equivalent on the EPR time scale. The crystallographic structures of the bis(μ-oxo)-Mn^{III}-Mn^{IV} nitrogenous complexes of bipyridyl,[10] CYCLAM,[13] and TMPA[14] are also consistent with the trapped valence since Mn^{IV} is readily differentiated from Mn^{III} in them by its shorter metal-ligand bond lengths. The d^4 Mn^{III} is additionally capable of a Jahn-Teller distortion that makes its $d_{x^2-y^2}$ and d_{z^2} orbitals and their respective bond lengths inequivalent.[21] The Jahn-Teller distortion gives an explanation for why the bonds to the axial ligands on Mn^{III} (i.e., those manganese-nitrogen bonds approximately perpendicular to the Mn^{III}-bis(μ-oxo)-Mn^{IV} plane and starred in Figure 1) are longer by at least 0.2 Å than the bonds to the in-plane nitrogen and oxygen ligands.[10,13,14]

Although these bis(μ-oxo)-Mn^{III}-Mn^{IV} models certainly may differ in their explicit nitrogen-containing, metal-liganding environment from the ultimate detailed structure of the coupled manganese in the OEC, the X-ray structure of the models studied here has, together with its nitrogenous liganding environment shown in Figure 1, been thoroughly elucidated.[13,14] These models give a definitive structural starting point for correlating structure with hyperfine couplings, spin densities, and underlying electronic

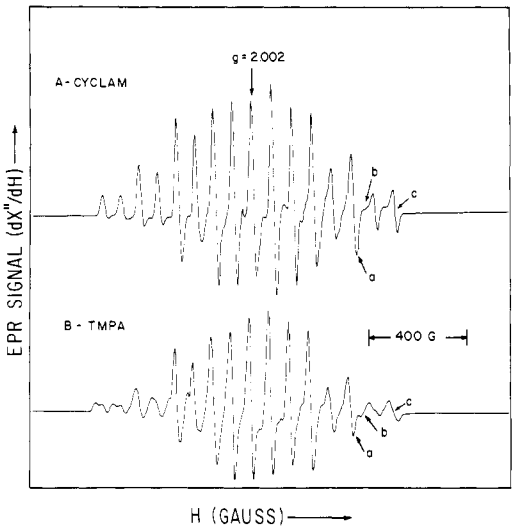

Figure 2. EPR spectra of the bis(μ-oxo)-Mn^{III}-Mn^{IV} complexes of (A) CYCLAM and (B) TMPA. These spectra were taken at T = 4.2 K with a microwave power of 1 μW and field modulation of 4 G ptp, and each trace represents four accumulations of data over a 2000-G range in a collection time of 50 s/accumulation. The EPR frequency was 9.219 GHz for the CYCLAM complex and 9.181 GHz for the TMPA complex. The letters a and b indicate where ENDOR spectra in this paper were obtained and c where the PFSEPR spectra were obtained.

structure. The hyperfine couplings, except for those of the manganese nuclei themselves, are not obvious from EPR spectra and must be elucidated with higher resolution techniques such as ESEEM,[22,23] ENDOR, and PFSEPR.

Materials and Methods

Materials. Bis(μ-oxo)-Mn^{III}-Mn^{IV} TMPA, which is $[Mn_2(TMPA)_2O_2](ClO_4)_3$, whose structure has previously been reported in the dithionate form,[14] was prepared according to a procedure somewhat different from that of ref 14. In the first step, $[Mn(TMPA)_2](ClO_4)_2$ was prepared as follows: The ligand TMPA[24] (1.63 g, 5.62 mmol) in methanol solution (25 mL) was added to a methanol solution (75 mL) of $Mn(ClO_4)_2{\cdot}6H_2O$ (1.00 g, 2.76 mmol). The mixture was stirred 3–4 h and filtered. Ether (100 mL) was then added with stirring to precipitate a white powder, which was filtered and washed first with a 20-mL methanol/ether (1/1) mixture and then with 20 mL of ether and dried in air for a yield of 2.15 g (93.4%) of $[Mn(TMPA)_2](ClO_4)_2$. Anal. Calcd for $C_{36}H_{36}Cl_2MnN_8O_8$: C, 51.80; H, 4.32; N, 13.43. Found: C, 51.72; H, 4.31; N, 13.38. Next, to a methanol solution (50 mL) of $[Mn(TMPA)_2](ClO_4)_2$ (1.67 g, 2.0 mmol), 2.0 mL of 30% aqueous H_2O_2 was added dropwise with stirring. Green microcrystalline solid precipitated over 5–10 min. After filtration, the precipitate was washed with 15 mL of methanol and dried to yield 0.95 g (93%) of $[Mn_2(TMPA)_2O_2](ClO_4)_3$. Anal. Calcd for $C_{36}H_{36}Cl_3Mn_2N_8O_{14}$: C, 42.34; H, 3.53; N, 10.98. Found: C, 42.29; H, 3.61; N, 11.02.

Bis(μ-oxo)-Mn^{III}-Mn^{IV} CYCLAM, which is $[Mn_2(CYCLAM)_2O_2](ClO_4)_3$, was prepared and crystallized according to the procedures of refs 12 and 13.

These samples were dissolved at room temperature in 1:1 DMF–methanol, which formed a glassy matrix upon freezing in liquid nitrogen. For an ENDOR check of exchangeable protons, a deuterated solvent consisting of 1:1 deuterated DMF–deuterated methanol (Merck 99.9% deuterated) was used. ENDOR samples were 1 mL in volume and approximately 1 mM in the appropriate bis(μ-oxo)-Mn^{III}-Mn^{IV} complex.

Methods. ENDOR measurements were done on a previously described homemade X-band EPR-ENDOR spectrometer at pumped liquid helium temperatures.[25,26] When nuclear spins are hyperfine coupled to electron spins, the ENDOR technique monitors the change in the EPR

(17) Fronko, R. M.; Penner-Hahn, J. E.; Bender, C. J. *J. Am. Chem. Soc.* **1988**, *110*, 7554–7556.
(18) Sands, R. H.; Dunham, W. R. *Q. Rev. Biophys.* **1975**, *7*, p 487.
(19) Diril, H.; Chang, R-H.; Nilges, M. J.; Zhang, X.; Potenza, J. A.; Schugar, H. J.; Isied, S. S.; Hendrickson, D. N. *J. Am. Chem. Soc.* **1989**, *111*, 5102–5114.
(20) Hush, N. S. *Prog. Inorg. Chem.* **1967**, *8*, 391–444.
(21) Cotton, F. A.; Wilkinson, G. *Advanced Inorganic Chemistry*, 4th ed.; Wiley: New York, 1980; pp 678–682.
(22) Britt, R. D.; Zimmermann, J-L.; Sauer, K.; Klein, M. P. *J. Am. Chem. Soc.* **1989**, *111*, 3522–3532.
(23) Britt, R. D. Ph.D. Thesis, Department of Physics, University of California at Berkeley, 1988.
(24) Anderegg, G.; Wenk, F. *Helv. Chim. Acta* **1967**, *50*, 2330–2332.
(25) Scholes, C. P. In *Multiple Electron Resonance Spectroscopy*; Dorio, M., Freed, J. H., Eds.; Plenum Press: New York, 1979; pp 297–328.
(26) Scholes, C. P.; Falkowski, K. M.; Chen, S.; Bank, J. F. *J. Am. Chem. Soc.* **1986**, *108*, 1660–1671.

signal that results when these nuclei are flipped by a radio frequency field.[25]

This magnetic resonance system was also modified for pulsed saturation recovery EPR[27] and for pulse field-sweep EPR (PFSEPR).[28,29] The pulse field-sweep EPR technique is a low-power technique for revealing hyperfine couplings from an inhomogeneously broadened EPR line and is complementary to ENDOR. In PFSEPR forbidden (spin-flip) transitions, where electron and nuclear spins simultaneously flip, are first excited and discretely saturated by a microwave pulse. Satellite holes (i.e., regions of microwave pulse saturation) due to these forbidden transitions are then detected at low, nonsaturating microwave powers during a field sweep about the field where the saturating pulse was applied. The splittings of these satellite features from each other and from the field where the initial microwave saturating pulse occurred give hyperfine,[28,29] and in some instances quadrupole,[29] couplings. For both ENDOR and PFSEPR measurements, a low-noise 15-dB GASFET amplifier was placed just prior to the microwave detector.

Results

EPR Results. Both CYCLAM and TMPA complexes gave 16-line EPR spectra in Figure 2 similar to those reported previously for bis(μ-oxo)-Mn^{III}-Mn^{IV} complexes.[11,13] Positions a and b of Figure 2 indicate where a number of ENDOR spectra shown below were taken and position c where PFSEPR spectra shown below were taken. The line shape of the two highest field features in the CYCLAM complex is similar to a shape that, for the bipyridyl complex of ref 11, indicated $g_{\parallel}$, $g_{\perp}$ anisotropy.

ENDOR Results. ENDOR spectra appeared from nitrogen in the 1–11-MHz region and from protons in the 11–22-MHz region. The proton features centered at the free proton NMR frequency near 16 MHz.

For ^{14}N ($I = 1$), the first-order spin Hamiltonian along a "z" direction is[25,30]

$$\mathcal{H} = AI_z\mathbf{s}_z + \tfrac{3}{4}(e^2Qq_{zz})[I_z^2 - \tfrac{1}{3}I(I+1)] - {}^{14}g_n\beta_n I_z H \quad (1)$$

where z is the direction of the applied magnetic field, H; A is the z component of hyperfine coupling; I_z and $\mathbf{s}_z$ are the nuclear and electron spin operators. Here $\mathbf{s} = {}^1/_2$ for the spin of the entire complex so that $\mathbf{s}_z$ has eigenvalues of $\pm{}^1/_2$. e^2Qq_{zz} is the first-order quadrupolar coupling along the z direction, where Q is the nuclear quadrupole moment and q_{zz} is the electric field gradient along the z direction. $^{14}g_n$ is the ^{14}N nuclear g value (=0.403), and β_n is the nuclear Bohr magnetron.

The first-order expressions for ENDOR frequencies are[25,30]

$$h\nu_{ENDOR} = \tfrac{1}{2}A \pm \tfrac{3}{4}(e^2Qq_{zz}) \pm {}^{14}g_n\beta_n H \quad (2)$$

A distinguishing characteristic of such ^{14}N features is that to first order they occur in pairs split by $2^{14}g_n\beta_n H/h$, or twice the ^{14}N nuclear Zeeman frequency, $^{14}\nu$, where $^{14}\nu = {}^{14}g_n\beta_n H/h$. In our experience, there are cases where Zeeman-split pairs are not well resolved or, especially for the lower frequency Zeeman pair, where their intensity is weak.[26,31] In ENDOR of low-spin ferric heme and histidine nitrogen,[26] we have found that the ^{14}N ENDOR features occurring below 2 MHz were often the ones most likely to have their frequencies deviate from first-order explanations. Such low-frequency ENDOR transitions arise from energy levels that are closer together, more nearly degenerate, and subject to broadening and state mixing from second-order quadrupolar or hyperfine interactions.

In Figure 3A,B nitrogen ENDOR features from the CYCLAM and the TMPA complexes are shown as they were as resolved at position a in Figure 2, and ^{14}N nuclear Zeeman frequency differences equal to twice the ^{14}N nuclear Zeeman frequency are denoted by arrows. The frequencies of the nitrogen ENDOR features and the calculated first-order hyperfine and quadrupolar couplings are listed in Table I. The lowest frequency feature of the CYCLAM complex, reported as a shoulder at 1.96 MHz in Table I, is less than twice the ^{14}N Zeeman frequency below the feature at 3.48 MHz. For the CYCLAM complex, we believed it most appropriate to use the three higher frequency features at 3.48, 5.81, and 7.94 MHz to calculate the quadrupolar and hyperfine couplings.

At position b for both CYCLAM and TMPA complexes, the features in the 6–9-MHz region were highly evident but somewhat broadened, while the features in the 1–4-MHz region were hard to resolve. The ENDOR features in the 6–9-MHz region continued to be observed at many fields across the EPR spectra of Figure 2 although not always with as good resolution as in Figure 3A,B. These 6–9-MHz features did *not* move with magnetic field

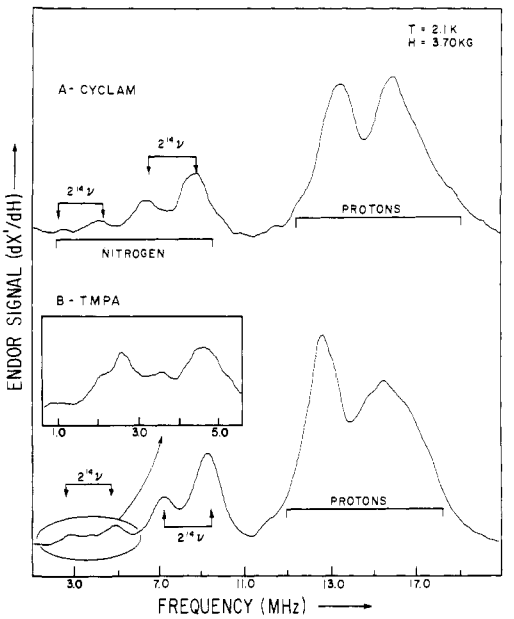

Figure 3. ENDOR features in the 1–23-MHz range from the bis(μ-oxo)-Mn^{III}-Mn^{IV} derivatives in deuterated solvent from (A) CYCLAM and (B) TMPA. These spectra were taken as position a in Figure 2 at 2.1 K. Microwave power was approximately 1 μW, ENDOR rf was approximately 0.5 G ptp, and 100-KHz field modulation was approximately 1.2 G ptp. The frequency sweeps were done at 2 MHz/s, and each spectrum represents 32 accumulations. The arrows labeled $2^{14}\nu$ point out frequency differences of twice the ^{14}N nuclear Zeeman splitting. The inset indicates additional details observed by slower frequency sweeps in the 1–5-MHz region from the TMPA complex.

Table I. Nitrogen ENDOR

compd	ENDOR frequencies[a,b] (MHz)	first-order couplings (MHz)
CYCLAM[d]	1.96 ± 0.15 sh	$\|A\|$ = 9.23 ± 0.13[c]
	3.48 ± 0.10	
	5.81 ± 0.10	$\|e^2Qq\|$ = 2.98 ± 0.12[c]
	7.94 ± 0.15	
TMPA[e]	2.27 ± 0.10	$\|A\|$ = 11.20 ± 0.10
	4.39 ± 0.10	
	6.80 ± 0.05	$\|e^2Q_q\|$ = 3.02 ± 0.12
	8.94 ± 0.05	

[a] Uncertainties in frequencies are estimated from the noise-related uncertainty in peak position. [b] Arrows indicate splittings of approximately $2^{14}g_n\beta_n H = 2^{14}\nu$. [c] These estimates were obtained under the assumption that peaks at 7.94, 5.81, and 3.48 correspond to first-order ENDOR frequencies of $A/2 + {}^3/_4e^2Qq + {}^{14}\nu$, $A/2 + {}^3/_4e^2Qq - {}^{14}\nu$, and $A/2 - {}^3/_4e^2Qq + {}^{14}\nu$ and the shoulder at 1.96 does not have its frequency well described by first-order theory since its separation from the 3.48-MHz feature is $<2^{14}\nu$. If we include the feature at 1.96 MHz in the calculation of $|A|$ and $|e^2Qq|$, we determine that $|A|$ = 9.60 and $|e^2Qq|$ = 2.78 MHz for CYCLAM. [d] H = 3.69 kG, position a, Figure 2A, $2^{14}g_n\beta_n H$ = 2.26 MHz. [e] H = 3.70 kG, position a, Figure 2B, $2^{14}g_n\beta_n H$ = 2.27 MHz.

(27) Scholes, C. P.; Janakiraman, R.; Taylor, H.; King, T. E. *Biophys. J.* **1984**, *45*, 1027–1030.
(28) Falkowski, K. M.; Scholes, C. P.; Taylor, H. *J. Magn. Reson.* **1986**, *68*, 453–468.
(29) Fan, C.; Taylor, H.; Bank, J. F.; Scholes, C. P. *J. Magn. Reson.* **1988**, *76*, 74–80.
(30) Scholes, C. P.; Lapidot, A.; Mascarenhas, R.; Inubushi, T.; Isaacson, R. A.; Feher, G. *J. Am. Chem. Soc.* **1982**, *104*, 2724–2735.
(31) Mulks, C. F.; Scholes, C. P.; Dickinson, L. C.; Lapidot, A. *J. Am. Chem. Soc.* **1979**, *101*, 1645–1654.

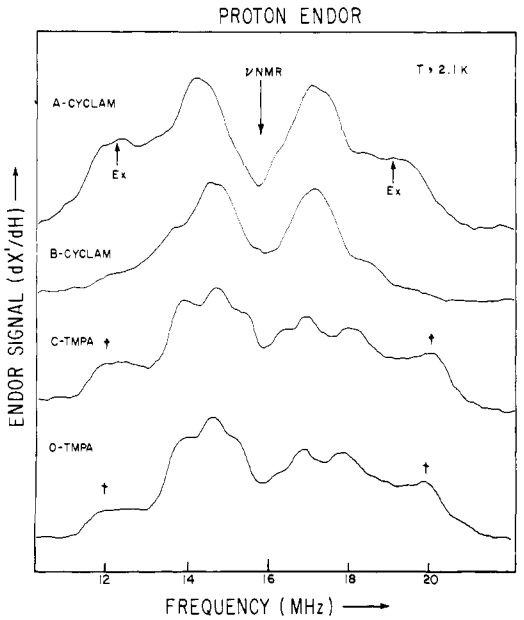

Figure 4. Proton ENDOR features centered about the free proton frequency near 16 MHz. (A) and (B) are from the CYCLAM derivative respectively in protonated and deuterated solvents and were obtained at position a in Figure 2. The peaks marked Ex were the exchangeable protons of the CYCLAM complex. (C) and (D) are from the TMPA derivative respectively in protonated and deuterated solvents and were obtained at position b in Figure 2. The peaks marked with daggers were found to have hyperfine couplings of about 8 MHz. Spectra were obtained at a microwave power of 1 μW, field modulation of 1.2 G ptp, ENDOR rf of 0.5 G ptp, and a frequency sweep rate of 1.2 MHz/s. Each trace represents about 16 accumulations of 10 s each.

(and free proton NMR frequency) as would be expected for protons; an implication of this behavior was that the nitrogen hyperfine coupling appeared to be largely isotropic. Quadrupolar and any anisotropic hyperfine interactions would, and apparently did, convolute with g anisotropy to broaden the ENDOR line shape at some magnetic fields.

On closer observation in the 1–5-MHz region of the TMPA complex, we detected a number of weaker low-frequency features, shown in the inset of Figure 3; it is possible that some of these features may be related to the nitrogen(s) with hyperfine coupling of 2.8 MHz obtained by ESEEM from Mn^{III}–Mn^{IV} models as mentioned in refs 22 and 23. We were thus concerned that the lower frequency (<5 MHz) features listed in Table I might not be from the same nitrogens as those which gave features at frequencies >5 MHz. However, the ENDOR results and the PFSEPR results (below) are mutually consistent in that they both arise from nitrogen(s) having a coupling of order 10 MHz.

Proton ENDOR Results. Proton results are phenomenologically explained by a spin Hamiltonian formally similar to that of eq 1, except that there is no quadrupole term. The first-order expression for proton ENDOR frequencies is

$$h\nu_{ENDOR} = h^{p}\nu_{NMR} \pm \tfrac{1}{2}A \qquad (3)$$

where ${}^{p}\nu_{NMR} = {}^{p}g_n\beta_n H/h$ is the free proton NMR frequency, ${}^{p}g_n = 5.585$, and A is a proton hyperfine coupling. Proton hyperfine coupling may be due to directly transferred electron spin density residing at the proton nucleus or to dipolar coupling through space between an electron spin localized at the metal and a distant proton. This latter dipolar interaction has been observed quantitatively to account for hyperfine coupling between heme iron in aquometmyoglobin and exchangeable protons of the water ligand.[31]

The proton ENDOR spectra are shown for the CYCLAM complex in Figure 4A,B and for the TMPA complex in Figure 4C,D. Figure 4A,C was from samples in protonated solvent while 4B,D was from samples in deuterated solvent. The best resolved proton spectrum from the CYCLAM complex came at the same

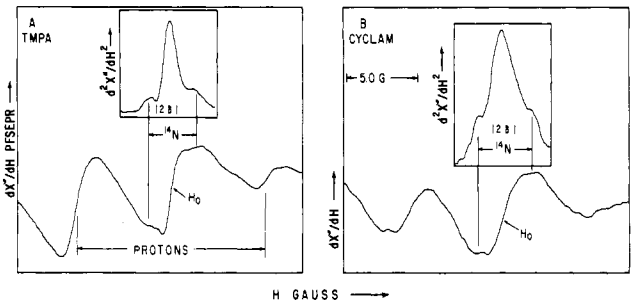

Figure 5. PFSEPR spectra showing nitrogen couplings from (A) the TMPA derivative and (B) the CYCLAM derivative. For these spectra a microwave pulse of approximately 1.3 mW and of duration 0.1 ms was followed by a field sweep over a range of approximately ±13 G about the original field position and at a microwave power during the sweep that was attenuated by 40 dB from the pulse power. The field sweep took 20 ms. H_0 denotes the position of the initial microwave pulse, and H_0 here was approximately 3.87 kG. 2δ is the splitting between the nitrogen PFSEPR features. Each spectrum was obtained from about 4000 0.02-s traces. The temperature was 1.5 K. The insets show second-derivative spectra, numerically computed from the first-derivative field-modulated PFSEPR spectra, to enhance the ^{14}N features.

EPR line position (a in Figure 2A) where the nitrogen ENDOR was best resolved. This spectrum clearly shows exchangeable protons with coupling of 6.7 ± 0.7 MHz; these features from the CYCLAM complex became broadened and less resolved when we went to position b in Figure 2A. The best resolved proton spectrum for the TMPA complex occurred at position b in Figure 2B, and from the TMPA complex there was no evidence at any of the EPR line positions for exchangeable proton ENDOR. The largest splittings measured from the TMPA complex, denoted with daggers in Figure 4C,D, were approximately 8.0 ± 0.5 MHz.

Pulse Field-Sweep EPR. A purpose of taking PFSEPR spectra was to confirm nitrogen hyperfine couplings. For nitrogen, the PFSEPR splittings, δ, in gauss away from the central hole are expected to be[28]

$$\delta = \pm[A/2 \pm {}^{14}g_n\beta_n H \pm \tfrac{3}{4}e^2Qq_{zz}]/g_e\beta \approx \pm A/(2g_e\beta_e) \qquad (4)$$

At $g_e = 2$, a splitting of 1 G translates into 2.8 MHz in frequency units. For PFSEPR of low-spin ferric heme and imidazole nitrogens, the small quadrupole and nuclear Zeeman terms remained unresolved,[28] and these terms remained unresolved here although they broaden the PFSEPR features. Proton spin-flip transitions[28] were also observed here, whose splitting is related to the free proton NMR frequency and is $\pm{}^{p}\nu/(g_e\beta_e)$.

The TMPA complex gave the best resolved, standard first-derivative presentation[28] of PFSEPR splittings, labeled in Figure 5A. Better resolution of the PFSEPR splittings, which are really shoulders in the first-derivative presentation, were obtained from both CYCLAM and TMPA complexes by taking a second derivative. The primary nitrogen PFSEPR features have splittings of $\pm\delta$ away from the center at H_0. For the CYCLAM and TMPA complexes, values of 2δ are 3.2 ± 0.6 G, or 9.0 ± 1.8 MHz. Since ESEEM measurements have reported a weak hyperfine coupling of 2.8 MHz from Mn^{III}–Mn^{IV} models,[22,23] we were concerned that the two lower frequency nitrogen ENDOR features in Figure 3 below 5 MHz for either the CYCLAM or TMPA complexes might be from altogether different nitrogens than those in the 6–9-MHz region. If the nitrogen ENDOR features in the 6–9-MHz region were unrelated to the features below 5 MHz, their hyperfine coupling would be of order 15 MHz and not of order 10 MHz. However, there is agreement between the hyperfine couplings directly determined from PFSEPR, but with relatively low resolution, and the couplings determined after application of eq 2 to the higher resolution ENDOR data. This agreement is definitive experimental evidence that the observed ENDOR features reported in Table I are for each respective complex all from the same type of nitrogen and that this type of nitrogen has the coupling indicated in Table I.

Although the manganese hyperfine couplings were well resolved by EPR, we have also used PFSEPR to verify the smaller coupling

of order 80 G to Mn^{IV}.[11,13] Splittings due to forbidden transitions at approximately ±40 G away from the central PFSEPR hole were observed. These splittings were not simply a reproduction of the EPR splittings since, as expected for the PFSEPR hole-burning technique, they centered at the position where the hole was burned.[28,29] This work points to future utility of the PFSEPR technique in resolving less obvious metal nuclear hyperfine couplings, as has already been done with copper proteins.[29]

Discussion

The hyperfine couplings that we experimentally measured by ENDOR are straightforwardly related to the phenomenological spin Hamiltonian of eq 1, and this spin Hamiltonian is written in terms of the cluster spin, $\mathbf{s} = {}^1/_2$. For a detailed understanding of spin densities and for later comparison to other non-Mn^{III}-Mn^{IV} systems, we must convert these phenomenological couplings in the cluster to couplings that would be measured for nuclei near hypothetical isolated Mn^{III} or Mn^{IV} ions.[11,18,19] In the binuclear cluster, the spin operators $\mathbf{s}_1 = 2$ for Mn^{III} and $\mathbf{s}_2 = {}^3/_2$ for Mn^{IV} add vectorially to yield the total spin, $\mathbf{s} = {}^1/_2$, of the complex. The component spins, $\mathbf{s}_1$ and $\mathbf{s}_2$, are quantized along this total spin.

If A_1 and A_2 are hyperfine couplings measured for nitrogen ligands respectively attached to Mn^{III} and Mn^{IV} *in the cluster*, and A_1' and A_2' are the corresponding couplings to the hypothetical isolated ions, it can be shown that $A_1 = A_1'(\mathbf{s}_1\cdot\mathbf{s}/\mathbf{s}^2)$ and $A_2 = A_2'(\mathbf{s}_2\cdot\mathbf{s}/\mathbf{s}^2)$.[11,18,19] Thus

$$A_1 = 2A_1' \text{ (for Mn}^{III}\text{)} \qquad A_2 = -A_2' \text{ (for Mn}^{IV}\text{)} \qquad (5)$$

Such a relation has explained why the effective hyperfine couplings to the manganese nuclei of Mn^{III} and Mn^{IV} in the binuclear cluster are respectively about 160 and 80 G while the intrinsic couplings to isolated ($\mathbf{s}_1 = 2$) Mn^{III} and to ($\mathbf{s}_2 = {}^3/_2$) Mn^{IV} are both about 80 G.[11,19] If the nitrogen hyperfine coupling that we have observed by ENDOR was from nitrogens ligated to the Mn^{III}, the magnitude of the relevant "isolated ion" hyperfine coupling would be $A_1' = 4.62$ MHz for the CYCLAM complex and $A_1' = 5.60$ MHz for the TMPA complex.

Nitrogen Hyperfine Couplings. We give a justification for which nitrogen ligands are associated with the ENDOR spectra and what the spin densities are on these nitrogens. From expressions that relate hyperfine couplings to spin density in s or p orbitals[32] and from past experience,[26,30,31] we know that unpaired electron spin in a valence 2s orbital will give rise to an order of magnitude larger hyperfine coupling via an isotropic Fermi contact mechanism than the same amount of electron spin in a 2p orbital. A metal e_g orbital (here a d_{z^2} or $d_{x^2-y^2}$ orbital) will transfer unpaired spin via a metal to nitrogen directed σ bond into such a nitrogen 2s valence orbital. On the other hand, t_{2g} metal orbitals (here, d_{xy}, d_{yz}, d_{xz}) that π bond to ligands would not put spin density directly into a valence 2s orbital. Mn^{III} ($\mathbf{s}_1 = 2$) has four unpaired electrons, one in a σ-antibonding e_g orbital and three in π-bonding t_{2g} orbitals; Mn^{IV} ($\mathbf{s}_2 = {}^3/_2$) has three π-bonding t_{2g} orbitals. In Mn^{III} systems, a Jahn–Teller distortion removes the degeneracy of d_{z^2} and $d_{x^2-y^2}$ orbitals and leaves one of these e_g orbitals populated with an unpaired electron and possessing a longer Mn–nitrogen bond.[21] The longer Mn^{III}–nitrogen bond, which is known to be the axial one,[13,14] would therefore have the unpaired electron in its d_{z^2} antibonding orbital. *We therefore claim that the axial nitrogens on the Mn^{III}, which we star in Figure 1, should be the ones with significant Fermi couplings whose features we are observing by ENDOR.* All the rest of the nitrogens on both Mn^{III} and Mn^{IV} interact with unpaired metal spin only through π-bonding t_{2g} orbitals. The σ-bonding orbital for the secondary amine nitrogen is a tetrahedral sp^3, and the σ-bonding orbital for the pyridine nitrogen is a trigonal sp^2. Therefore, it is expected that the Fermi contribution for the amine nitrogen of CYCLAM should be about 75% of that of the pyridine nitrogen of TMPA; the experimental ratio of hyperfine couplings is 82%. An additional aspect that may cause the hyperfine coupling to the nitrogen of the CYCLAM complex to be less than that of the TMPA complex is that the average axial Mn^{III}–nitrogen bond length in the CYCLAM complex is 2.35[13] versus 2.23 Å for the TMPA complex.[14]

Having initially reduced the problem to couplings on hypothetical isolated metal complexes of spin 2 or ${}^3/_2$, we must still determine spin densities. Standard expressions exist to relate hyperfine coupling due to spin density at a ligand nucleus when the molecular orbital that contains this spin density is one individual orbital out of, say, $2\mathbf{s}_1$ orbitals centered on a metal complex of spin $\mathbf{s}_1$.[30,32] These expressions all multiply the coupling that would occur for the individual orbital if there had been only a single unpaired electron by a factor of $1/(2\mathbf{s}_1)$. Specifically, the Fermi contact interaction due to unpaired electron spin density in the σ-bonded nitrogen 2s orbital is

$$A'_{\text{Fermi}}\,(\text{MHz}) = (1/2\mathbf{s}_1)(16 \times 10^{-6}) f_s \beta_n \beta_e |\psi_{o2s}|^2/3h \qquad (6)$$

where f_s is the fraction of electron spin in the nitrogen 2s orbital, ψ_{o2s} is the 2s wave function at the nitrogen nucleus, $|\psi_{o2s}|^2 = 33.4 \times 10^{24}$ cm^{-3},[33,34] and $\mathbf{s}_1 = 2$ here. For the σ-bonded porphyrin sp^2 nitrogens of high-spin ferric heme and of cupric copper, the fractions of electron spin were respectively 2.5[30] and 3.0%.[35] If we assume that the intrinsic couplings of 4.62 and 5.60 MHz for CYCLAM and TMPA binuclear complexes are entirely due to Fermi contact interactions, then the fraction of 2s electron spin for each axial σ-bonded nitrogen here is about 1.2% for the CYCLAM and about 1.4% for the TMPA complex. These covalent contributions are about half those in the high-spin ferric and the cupric porphyrin compounds, whose metal–nitrogen bond distances of 2.04[36] and 1.98 Å[37] are 0.2–0.3 Å shorter than the Mn^{III}–nitrogen axial bonds.

We estimate as follows that the hyperfine coupling to the other nitrogens that interact only with π-bonding t_{2g} orbitals should be considerably less than 10 MHz. In low-spin ferric heme, which is an $\mathbf{s} = {}^1/_2$ system with a single π-bonding t_{2g} electron, the ^{14}N hyperfine coupling is of the order 6 MHz.[26] The coupling includes direct effects of π electrons and weak indirect Fermi coupling via exchange polarization of s orbitals.[26] The Fe–nitrogen bond distances in the ferric heme case are less than any of the Mn–nitrogen bond distances in our Mn^{III}–Mn^{IV} complexes.[13,14,38] Since the hyperfine coupling measured from an isolated metal complex with overall spin $\mathbf{s}_1 > {}^1/_2$ scales as $1/(2\mathbf{s}_1)$,[32] one would expect the corresponding couplings for the π-bonded nitrogens on an isolated $\mathbf{s}_1 = 2$ Mn^{III} to be of the order 1.5 MHz (=${}^1/_4$ of 6 MHz) and for isolated π-bonded nitrogens on the $\mathbf{s}_2 = {}^3/_2$ Mn^{IV} to be of the order 2 MHz (=${}^1/_3$ of 6 MHz). If the Mn^{III} and Mn^{IV} were then spin-coupled to each other, the exclusively π-bonding nitrogens on the Mn^{III} should have a coupling of the order 3 MHz (from eq 5) while the π-bonding nitrogens on the Mn^{IV} should have a coupling of the order (−)2 MHz. In either case, these small hyperfine couplings would be in the range where they are comparable with nitrogen Zeeman and quadrupolar interactions. Approximate equivalence of hyperfine, quadrupolar, and Zeeman interactions will lead to state mixing whence ENDOR features are broadened and not well explained by first-order expressions (eq 2). Whatever ENDOR features that are observed from exclusively π-bonded nitrogens would be expected to occur below about 5 MHz, as the weak additional features shown in the inset of Figure 3 do. When the nitrogen nuclear spin Hamiltonian has significant state mixing, ESEEM tends to give more tractable results. (When large hyperfine couplings exist and first-order expressions hold, ESEEM is not as effective as ENDOR.) Recent ESEEM from the OEC[22] and binuclear Mn^{III}–Mn^{IV} models[23] may indicate nitrogens with weak couplings less than 3 MHz. Such features may be π-bonded nitrogens on Mn^{III} or Mn^{IV}.

(32) Owen, J.; Thornley, J. H. M. *Rep. Prog. Phys.* **1966**, *29*, 675–728.
(33) Hartree, D. R.; Hartree, W. *Proc. R. Soc. London* **1949**, *A193*, 299–304.
(34) Maki, A. H.; McGarvey, B. R. *J. Chem. Phys.* **1958**, *29*, 35–38.
(35) Brown, T. G.; Hoffman, B. M. *Mol. Phys.* **1980**, *39*, 1073–1109.
(36) Koenig, D. F. *Acta Crystallogr.* **1965**, *18*, 663–673.
(37) Fleischer, E. B.; Miller, C. K.; Webb, L. E. *J. Am. Chem. Soc.* **1964**, *86*, 2342–2347.
(38) Collins, D. M.; Countryman, R.; Hoard, J. L. *J. Am. Chem. Soc.* **1972**, *94*, 2066–2078.

Nitrogen Quadrupolar Couplings. In solid pyridine and solid secondary amine, the ^{14}N nuclear quadrupole coupling constants, whose principal field gradient axis is along the lone pair, are respectively 4.584 and 4.650 MHz (ref 39, pp 235 and 221, respectively.) The quadrupolar couplings for the pyridine nitrogen of TMPA and the secondary amine nitrogen of CYCLAM in Mn^{III}–Mn^{IV}–bis(μ-oxo) complexes are respectively 3.02 and 2.98 MHz. If these couplings refer to the principle electric field gradient axis, then a decrease in electric field gradient on bonding to a metal would reflect transfer of lone pair electron density in bonding orbitals to the metal.[39] Such transfer would make the electronic environment of the nitrogen more symmetric and reduce the electric field gradient.

Proton Hyperfine Couplings. The coupling of proton uptake to electron transfer has been observed for the bis(μ-oxo)–Mn^{III}–Mn^{IV} bipyridyl complex.[40] The suggestion is that concomitant proton uptake and electron transfer by a binuclear Mn^{III}–Mn^{IV} center are relevant to the steps of the Kok S cycle.[2,40] The relation between proton uptake and electron transfer was a motivation to probe here for hyperfine coupling of the Mn^{III}–Mn^{IV} center to exchangeable protons. It is clear from the ENDOR spectra that there are exchangeable protons associated with the metal center(s) of the CYCLAM complex, while such exchangeable protons were not observed for the TMPA complex. The implication is that the exchangeable protons observed here are those protons on the secondary amine nitrogens, though, of course, these observations of exchangeability are no doubt dependent on the hydrogen-bonding strength of the methanol and DMF solvent. The TMPA macrocycle has no such exchangeable protons. If exchangeable protons had been observed from the TMPA complex, there would have been a good likelihood that they were protons hydrogen-bonded to the cross-linking μ-oxo groups.

The approximate distances to the amino nitrogens of the CYCLAM are 2–2.3 Å so that the Mn^{III} or Mn^{IV} to amino proton distances should be 3.0–3.5 Å. Given the small hyperfine coupling to the adjacent nitrogens, the amount of unpaired electron spin reaching these protons should be small. Thus, the hyperfine couplings to the amino protons should be dipolar and dependent as $1/R^3$ on the distance between a manganese and a proton. The dipolar coupling between an isolated metal spin and a proton can be calculated by standard formulas,[25,32] and then the hyperfine coupling to the isolated nucleus must be converted to hyperfine coupling within the Mn^{III}–Mn^{IV} complex by use of eq 5. If a proton is at a distance R from, say, spin s_1, then its dipolar hyperfine coupling (on the isolated metal) is

$$A_{1dip}' = g_e\beta_e g_n\beta_n(3\cos^2\theta - 1)/(hR^3) \qquad (7)$$

where θ is the angle between the applied magnetic field and the metal to proton vector. Then, with reference to the $s = {}^1/_2$ complex, $A_{1dip} = 2A_{1dip}'$ (for Mn^{III}) and $A_{2dip} = -A_{2dip}'$ (for Mn^{IV}). It is possible that a proton could be dipolar-coupled to both metals, but we neglect that possibility here since it would be most relevant only to protons hydrogen bonded to μ-oxo oxygens. For the dipolar expressions of eq 7, the extrema at $\theta = 0°$ and 90° will give rise to considerable ENDOR intensity. For a Mn–proton distance of 3.5 Å, the dipolar couplings at the $\theta = 0°$ and 90° turning points would be 1.8 and 3.6 MHz for Mn^{IV} and 3.6 and 7.2 MHz for Mn^{III}, while for a Mn–proton distance of 3.0 Å, the dipolar couplings at the $\theta = 0°$ and 90° turning points would be 2.8 and 5.9 MHz for Mn^{IV} and 5.6 and 11.8 MHz for Mn^{III}. The exchangeable proton coupling of 6.7 MHz in the CYCLAM complex implies that the protons being observed are on nitrogens ligated to Mn^{III}. The best resolution of these exchangeable protons occurred at the same field position where the nitrogen ENDOR was also best resolved so that it is possible that these protons are in fact hydrogen bonded to the axial nitrogens on the Mn^{III}. In the TMPA case, the largest couplings to nonexchangeable protons are likely to be those protons that are on pyridine carbons next to the nitrogens that ligate to the Mn^{III}.

Conclusions

This work gives detailed insight into the electronic structure of two antiferromagnetically coupled bis(μ-oxo)–Mn^{III}–Mn^{IV} nitrogenous models whose EPR signals are relevant to the PS II multiline signal of the oxygen-evolving center. TMPA provided three pyridyl nitrogens and one tertiary amino nitrogen as ligands for each metal ion, while CYCLAM provided four secondary amino nitrogens as ligands for each metal ion. Electron–nitrogen hyperfine coupling of order 10 MHz was observed by ENDOR and PFSEPR from nitrogen(s) of these complexes; the hyperfine coupling from the more precise ENDOR technique applied to the nitrogen(s) of the CYCLAM complex was about 80% of the coupling to the TMPA nitrogen(s). The nitrogen hyperfine coupling is due to a contact Fermi interaction with unpaired nitrogen 2s spin, and the primary nitrogen candidates for this interaction are the two axial nitrogen ligands of Mn^{III}. The axial Mn^{III}–nitrogen bonds are known to be longer than other bonds in these complexes because they contain a σ-antibonding e_g electron that happens to be unpaired. This e_g orbital, specifically a d_{z^2} orbital, will participate in a σ bond with 2s-containing orbitals on the nitrogen ligand. For TMPA, these are the sp^2 orbitals of the pyridyl nitrogens, and for CYCLAM these are the sp^3 orbitals of the secondary amines. (All other metal orbitals containing unpaired spin are of π-bonding t_{2g} symmetry.) From the CYCLAM complex, large hyperfine couplings of order 6.7 MHz were observed from exchangeable protons, and these are assigned as protons attached to secondary amino nitrogen ligands of the Mn^{III}. These exchangeable protons should be 3.0–3.5 Å away from the Mn^{III}. No such exchangeable protons were observed from the TMPA complex although proton ENDOR resonances due to covalently attached, nonexchangeable protons were observed from TMPA with couplings of up to 8 MHz.

Acknowledgment. This work was supported in part by NIH Grant GM 35103 (C.P.S.) and NSF Grant BBS 8711617 (C. P.S.). Acknowledgement is made to the donors of the Petroleum Research Fund, administered by the American Chemical Society, for partial support of this research (PRF Grant No. 19666-AC6 (C.P.S. and Y.G.)). We are grateful for useful discussion and advice from Prof. G. W. Brudvig and Prof. H. H. Thorp. Mr. H. Taylor gave us invaluable service in repair and modification of our EPR-ENDOR spectrometer, and we thank Ms. Janet F. Bank for help in sample preparation and careful attention to detail.

(39) Lucken, E. A. C. *Nuclear Quadrupole Coupling Constants*; Academic Press: New York, 1969; Chapters 7, 11.

(40) Thorp, H. H.; Sarneski, J. E.; Brudvig, G. W.; Crabtree, R. H. *J. Am. Chem. Soc.* **1989**, *111*, 9249–9250.